Nanoscale Advances

ROYAL SOCIETY OF CHEMISTRY

PAPER

View Article Online
View Journal | View Issue

Check for updates

Cite this: *Nanoscale Adv.*, 2025, **7**, 3676

# Synthesis, characterization, and evaluation of low molecular weight poly(β-amino ester) nanocarriers for enhanced T cell transfection and gene delivery in cancer immunotherapy†

Alireza Gharatape, [ab] Ali Sayadmanesh,[c] Hamid Sadeghi-Abandansari, [de] Hossein Ghanbari,[b] Mohsen Basiri *[cf] and Reza Faridi-Majidi *[abg]

Cancer immunotherapy represents a revolutionary approach in cancer treatment by leveraging the body's immune system to target and eliminate cancer cells. An emerging strategy within this field is gene delivery, which can enhance the efficacy of immune cells. Nanocarrier-based gene delivery methods have gained prominence due to their ability to protect and transport genetic material into cells efficiently. Polymeric nanocarriers, in particular, offer significant advantages, such as customizable physical and chemical properties, biocompatibility, and the potential for targeted delivery. Among polymeric nanocarriers, poly(β-amino ester) (PBAE) polymers are notable for their biodegradability, low cytotoxicity, and high gene transfection efficiency. This study investigates the synthesis and characterization of low molecular weight PBAE nanocarriers, assessing their potential in gene delivery applications for Jurkat and primary T cells—both crucial in cancer immunotherapy. Our research involved synthesizing PBAE polymer and creating nanocarriers at various DNA-to-polymer ratios. We characterized these nanocarriers in terms of size, zeta potential, and encapsulation efficiency. Confocal microscopy and flow cytometry were utilized to evaluate cellular uptake and transfection efficiency. The results demonstrated appropriate transfection efficiency and significant gene expression in both hard-to-transfect cell types (jurkat up to 37% and primary T cell 5%), with optimized DNA-to-polymer ratios showing minimal cytotoxicity. This study highlights the potential of PBAE nanocarriers in enhancing gene delivery for cancer immunotherapy. By effectively transfecting T cells, these nanocarriers could improve the therapeutic outcomes of immunotherapy, offering a promising pathway for developing more effective cancer treatments.

Received 18th February 2025
Accepted 1st May 2025

DOI: 10.1039/d5na00169b

rsc.li/nanoscale-advances

Open Access Article. Published on 02 Caxah Alsa 2025. Downloaded on 27/05/2026 6:00:34 PM.
This article is licensed under a Creative Commons Attribution-NonCommercial 3.0 Unported Licence.

## 1. Introduction

Cancer remains one of the leading causes of mortality worldwide, necessitating the development of innovative therapeutic strategies. Traditional treatments such as chemotherapy and radiation therapy, while effective to some extent, often come with significant side effects and limitations.[1,2] Immunotherapy, which harnesses the body's immune system to target and eliminate cancer cells, has emerged as a revolutionary approach in oncology.[3,4] Among the various immunotherapeutic strategies, the genetic engineering of T cells to express chimeric antigen receptors (CARs) or T cell receptors (TCRs) has shown remarkable clinical success in treating hematological malignancies.[5–7] However, the widespread application of these therapies is hindered by challenges related to the efficient and safe delivery of genetic material into T cells.[8,9] The genetic engineering of T cells involves the introduction of exogenous genetic material to modify their function or enhance their therapeutic potential. This process typically requires the

[a]*Advanced Laboratory of Nanocarriers Synthesis (ALNS), Department of Medical Nanotechnology, School of Advanced Technologies in Medicine, Tehran University of Medical Sciences, Tehran, Iran. E-mail: refaridi@sina.tums.ac.ir*

[b]*Department of Medical Nanotechnology, School of Advanced Technologies in Medicine, Tehran University of Medical Sciences, Tehran, Iran*

[c]*Department of Stem Cells and Developmental Biology and Cell Science Research Center, Royan Institute for Stem Cell Biology and Technology, Tehran, Iran. E-mail: mbasiri@coh.org*

[d]*Department of Cell Engineering, Cell Science Research Center, Royan Institute for Stem Cell Biology and Technology, ACECR, Tehran, Iran*

[e]*Department of Stem Cells and Developmental Biology, Faculty of Sciences and Advanced Technologies in Biology, University of Science and Culture, Tehran, Iran*

[f]*Department of Hematology & Hematopoietic Cell Transplantation (T Cell Therapeutics Research Laboratories), City of Hope Beckman Research Institute and Medical Center, Duarte, CA, USA*

[g]*Pharmaceutical Nanotechnology research center, Tehran University of Medical Sciences, Tehran, Iran*

† Electronic supplementary information (ESI) available. See DOI: https://doi.org/10.1039/d5na00169b



© 2025 The Author(s). Published by the Royal Society of Chemistry

Open Access Article. Published on 02 Caxah Alsa 2025. Downloaded on 27/05/2026 6:00:34 PM.
This article is licensed under a Creative Commons Attribution-NonCommercial 3.0 Unported Licence.

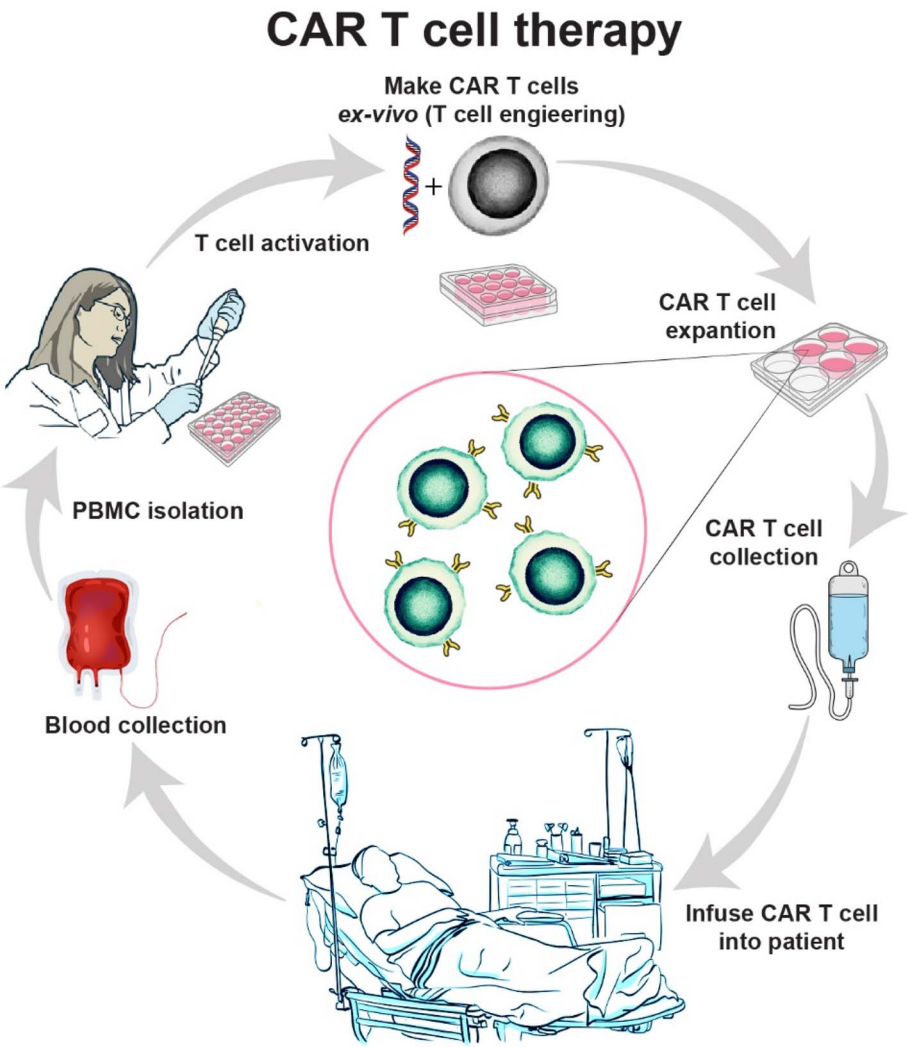


Fig. 1 The schematic illustration provides a visual overview of the key steps involved in CAR T cell therapy. The process begins with the collection of a patient's blood, from which peripheral blood mononuclear cells (PBMCs) are isolated. These PBMCs are then genetically engineered ex vivo to express chimeric antigen receptors (CARs), which are artificial T cell receptors designed to target specific antigens on cancer cells. The engineered T cells are expanded in culture to generate a sufficient number of cells for infusion back into the patient. Finally, the expanded CAR T cells are infused into the patient's bloodstream, where they circulate and target cancer cells expressing the specific antigen. This targeted therapy offers a promising approach for treating various types of cancer, particularly hematological malignancies.

delivery of plasmid DNA or mRNA encoding the desired gene (Fig. 1). The efficiency of gene transfer is a critical factor in determining the success of T cell engineering.[9,10]

The field of cancer immunotherapy has made remarkable progress in recent years, with the genetic engineering of immune cells emerging as a promising strategy for combating various malignancies.[11,12] Among the various approaches, the use of polymer nanocarriers for gene delivery has garnered significant attention due to their potential to enhance the efficacy and specificity of genetic modifications.[13,14] Polymeric nanocarriers have emerged as a promising solution to overcome the limitations associated with viral vectors, which are commonly used for gene delivery. Viral vectors, while highly efficient, pose risks such as insertional mutagenesis and immunogenicity.[15,16] Moreover, the treatment process based on these methods is very expensive.[17,18] In contrast, polymeric nanocarriers offer several advantages, including lower immunogenicity, ease of synthesis, and the ability to be tailored for specific applications.[19] In this context, poly (beta amino ester) (PBAE) polymers have emerged as a versatile and effective class of nanocarriers for gene transfer. The PBAEs have gained prominence due to their biodegradability, biocompatibility, and tunable properties.[20,21] These polymers can be synthesized through a simple and scalable process, allowing for the incorporation of various functional groups to enhance their gene delivery capabilities.

The synthesis of PBAE polymers involves the Michael addition reaction between primary amines and diacrylates, resulting in a diverse library of polymers with varying structures and properties.[22] This versatility allows for the optimization of PBAE polymers for specific gene delivery applications. PBAE polymers have been shown to form stable complexes with nucleic acids,

Open Access Article. Published on 02 Caxah Alsa 2025. Downloaded on 27/05/2026 6:00:34 PM.
This article is licensed under a Creative Commons Attribution-NonCommercial 3.0 Unported Licence.

facilitating their uptake by cells and subsequent expression of the transgene.[22] In this study, we optimized the formulation of PBAE nanocarriers to achieve efficient gene transfer to Jurkat cells and primary T cells, with a focus on minimizing cytotoxicity and maximizing transgene expression. The application of PBAE nanocarriers for gene delivery in cancer immunotherapy holds significant promise.[5,6,23] By enabling the efficient and safe genetic modification of T cells, these nanocarriers can enhance the efficacy of CAR T cell therapies and other adoptive cell transfer approaches. However, the manufacturing process for CAR T cells is complex and costly, limiting its accessibility to patients. The use of PBAE nanocarriers for *in vivo* gene delivery could simplify the production of CAR T cells and reduce the associated costs, making this therapy more widely available.

In addition to CAR T cell therapy, the genetic engineering of T cells using PBAE nanocarriers can be applied to other immunotherapeutic strategies. For example, T cells can be engineered to express TCRs that recognize tumor-specific antigens, enabling the targeted elimination of cancer cells.[5,24] Furthermore, the ability to deliver multiple genes simultaneously using PBAE nanocarriers opens up new possibilities for combination therapies, where T cells can be modified to express multiple therapeutic proteins that enhance their anti-tumor activity.[25–27]

These versatile polymers can be adapted for gene delivery in a wide range of applications, including the treatment of genetic disorders, infectious diseases, and autoimmune conditions.[28–30] The ability to tailor the properties of PBAE polymers through chemical modifications allows for the development of customized nanocarriers that meet the specific requirements of different therapeutic applications. In this study, we demonstrate the feasibility of using low molecular weight PBAE nanocarriers for the genetic engineering of T cells, providing a foundation for future research and development in this field. We synthesized low molecular weight PBAE polymer and evaluated their potential as nanocarriers for gene transfer to Jurkat cells and primary T cells. The choice of these cell types is particularly relevant, as Jurkat cells serve as a model for T cell leukemia, while primary T cells represent a more clinically relevant target for genetic engineering.

By leveraging the unique properties of PBAE polymer, we have investigated their efficiency in gene delivery to T cells, a crucial step in advancing genetic engineering approaches for immunotherapy. The findings of this study provide insights into optimizing PBAE-based transfection strategies for immune cells, potentially facilitating the future development of gene-modified T cell therapies.

# 2. Materials and method

## 2.1 Materials

The following materials and reagents were used in this study: 4-amino-1-butanol (CAS No. 13325-10-5, Sigma-Aldrich, USA), 1,4-butanediol diacrylate (CAS No. 1070-70-8, Sigma-Aldrich, USA), 1-(3-aminopropyl)-4-methyl-piperazine (CAS No. 120-20-7, Sigma-Aldrich, USA), tetrahydrofuran (THF) (CAS No. 109-99-9, Sigma-Aldrich, USA), diethyl ether (CAS No. 60-29-7, Sigma-Aldrich, USA), dimethyl sulfoxide (DMSO) (CAS No. 67-68-5, Sigma-Aldrich, USA), sodium chloride (NaCl) (CAS No. 7647-14-5, Sigma-Aldrich, USA), hydrochloric acid (HCl) (CAS No. 7647-01-0, Sigma-Aldrich, USA), sodium hydroxide (NaOH) (CAS No. 1310-73-2, Sigma-Aldrich, USA), heparin (CAS No. 9041-08-1, Sigma-Aldrich, USA), and Gel-Red fluorescent dye (Biotium, USA, Catalog No. 41003).

For cell culture, RPMI-1640 medium (Gibco, Thermo Fisher Scientific, USA, Catalog No. 11875093), GlutaMax supplement (Gibco, Thermo Fisher Scientific, USA, Catalog No. 35050061), fetal bovine serum (FBS) (Gibco, Thermo Fisher Scientific, USA, Catalog No. 16000044), and Opti-MEM medium (Gibco, Thermo Fisher Scientific, USA, Catalog No. 31985062) were used. Interleukin-2 (IL-2) (R&D Systems, USA, Catalog No. 202-IL) was used for T-cell culture.

Antibodies included anti-CD3 (Miltenyi Biotec, Germany, Catalog No. 130-093-387) and anti-CD28 (Miltenyi Biotec, Germany, Catalog No. 130-093-375). Assay kits and tools included the Quant-iT dsDNA High-Sensitivity Assay Kit (Invitrogen, USA, Catalog No. Q32854) and a Qubit Fluorometer (Invitrogen, Thermo Fisher Scientific, USA).

Instrumentation used in the study included a Bruker NMR spectrometer (400 MHz, Bruker Corporation, USA), Malvern Zetasizer Nano ZS (Malvern Instruments, UK), Zeiss EM900 transmission electron microscope (Carl Zeiss AG, Germany), Leica TCS SP8 confocal laser scanning microscope (Leica Microsystems, Germany), Olympus IX71 fluorescence microscope (Olympus Life Science, Japan), QUANTUM-ST4-1100/20 M transilluminator (Vilber Lourmat, France), and a Multiskan Spectrum microplate reader (Thermo Fisher Scientific, USA).

Additional materials included carbon-coated copper grids for TEM (Electron Microscopy Sciences, USA, Catalog No. CF400-Cu), aluminum grids for SEM (Electron Microscopy Sciences, USA, Catalog No. CF200-Al), and Ficoll solution (GE Healthcare, USA, Catalog No. 17-1440-02).

## 2.2 Synthesis and characterization of poly(β-amino ester) polymer

The synthesis of PBAE polymer was conducted *via* a two-step Michael addition polymerization. Initially, 4-amino-1-butanol (an amine monomer) was reacted with 1,4-butanediol diacrylate (a diacrylate monomer) at a molar ratio of 1.1 : 1 (acrylate to amine). This solvent-free reaction was performed in a glass vial with magnetic stirring at 90 °C in the absence of light for 24 hours. Subsequently, the base polymer was end-capped with 0.5 M of 1-(3-aminopropyl)-4-methyl-piperazine (an amine-containing small molecule) at a concentration of 625 mg $ml^{-1}$. This reaction took place in 8 mL of tetrahydrofuran (THF) under magnetic stirring at room temperature for 2 hours. Randomization in sample preparation was not necessary; however, all polymer characterizations were conducted in a blinded manner.

Upon completion of both reaction steps, the product was subjected to cold diethyl ether precipitation twice to eliminate any unreacted monomers. The final polymer was dried under vacuum at room temperature for 48 hours to remove residual


© 2025 The Author(s). Published by the Royal Society of Chemistry

Open Access Article. Published on 02 Caxah Alsa 2025. Downloaded on 27/05/2026 6:00:34 PM.
This article is licensed under a Creative Commons Attribution-NonCommercial 3.0 Unported Licence.

diethyl ether. The purified product was then dissolved in dimethyl sulfoxide (DMSO) at a concentration of 100 mg $mL^{-1}$ and stored with desiccant at −20 °C until further use. Structural characterization was performed using proton nuclear magnetic resonance ($^1$H NMR) spectroscopy, utilizing a Bruker spectrometer operating at 400 MHz in DMSO. The resulting spectra are shown in Fig. S1.† Final polymer structure and H-NMR analysis depicted in Fig. S2.†

The buffering capacity of the synthesized polymer was evaluated through acid-base titration. Ten microliters of the polymer solutions (PBAE and PEI) were diluted in 10 mL of 0.1 M sodium chloride (NaCl) solution. The pH of this solution was initially adjusted to 3 using 1 M hydrochloric acid (HCl). The solution was then titrated with 0.1 M sodium hydroxide (NaOH) until the pH reached 11. A Mettler Toledo S20 pH meter was used to measure the pH after each addition of NaOH. Two methods were employed to calculate the buffering capacity. The first method determined the ratio of total protons buffered within the physiological pH range (pH 7.4 to 5.1) to the total amine content of the polymer, assessing the efficiency of the polymer's amine groups in buffering within the physiological range. The second method used the same pH range but considered the ratio of buffered protons to the total polymer mass, providing a broader perspective on the overall buffering capacity. A control titration with 0.1 M NaCl solution without the polymer was also performed to account for any potential background effects from the salt solution.

In our study, NMR was employed to analyze the molecular weight distribution of polymers. This method enabled the determination of the mean repeat unit of the polymer (molecular weight = 287.36 g $mol^{-1}$) through the analysis of the area ratio between the peak corresponding to the terminal secondary amine hydrogen (1.7 ppm) and the α-carbon hydrogens of the diacrylate repeat units (4.01 ppm) (Fig. S2†). Based on this analysis, the molecular number was 10.4 and the molecular weight of the synthesized polymer was determined to be between 3 and 3.5 kDa, classifying it as a low molecular weight polymer.

### 2.3 Polyplex nanocarriers size and zeta potential

Poly(β-amino ester) (PBAE) polyplexes were synthesized at various polymer-to-DNA mass ratios (weight/weight (w/w) ratios), 1 : 15, 1 : 20, and 1 : 30. These formulations were prepared in sodium-acetate buffer (NaAc) at pH 5. To form the polyplexes at each N/P ratio, equal volumes (1 : 1 v/v) of polymer solution and plasmid solution were mixed and incubated for 10 minutes. Post-incubation, the complexes were diluted in 1× PBS (pH 7.4) for dynamic light scattering (DLS) analysis. The preparation steps were conducted in a blinded fashion to reduce bias, and measurements were performed in triplicate to ensure accuracy.

The particle size distribution and zeta potential of the polyplexes were determined using a Malvern Zetasizer Nano ZS instrument (Malvern Instruments, UK) at a detection angle of 173° and a wavelength of 633 nm. Measurements were conducted in triplicate. For size distribution analysis, the nanocarrier solution was diluted fivefold with PBS, whereas a 15-fold dilution was used for zeta potential measurements. Mean values and standard errors of the mean (SEM) were calculated for all measurements.

### 2.4 Transmission electron microscopy

Transmission electron microscopy (TEM) was utilized to visualize the polyplex nanocarriers. A Zeiss EM900 microscope (Carl Zeiss AG, Germany) was employed for this purpose. TEM analysis focused on nanocarriers encapsulating DNA prepared at a 1 : 20 N/P ratio. Twenty microliters of the unstained nanocarrier solution were placed onto carbon-coated copper grids and allowed to dry completely before imaging. Replication in imaging experiments was achieved by preparing three independent samples, ensuring reproducibility.

### 2.5 Scanning electron microscopy-energy dispersive X-ray spectroscopy

Scanning Electron Microscopy (SEM) combined with Energy Dispersive X-ray Spectroscopy (EDS) was used to examine the surface morphology and elemental composition of materials at high magnifications. SEM provides detailed images of the sample's surface, while EDS detects and maps the elemental distribution, offering comprehensive insight into the material's structure and composition. The nanocarriers were formed in a w/w ratio of 1 : 15. Then, twenty microliters of the unstained nanocarrier solution were placed onto aluminum grids and allowed to dry completely in a vacuum before imaging.

### 2.6 Polyplex nanocarriers formation and stability

A gel retardation assay was performed to determine the optimal DNA-to-polymer concentration ratio and incubation time for effective DNA complexation. This assay utilized 1% agarose gels containing 40 nL $mL^{-1}$ Gel-Red fluorescent dye. Nanoparticles were formed using DNA at a concentration of 500 ng $\mu L^{-1}$ and various DNA to polymer w/w ratios of 1 : 15, 1 : 20, and 1 : 30. The DNA and polymer solutions were allowed to complex for 5, 10, 15, or 20 minutes. The gels were run for 30 minutes at 120 V and visualized using a QUANTUM-ST4-1100/20 M trans-illuminator (Vilber Lourmat, France).

The integrity of the polyplexes, specifically their stability and ability to retain plasmid DNA (pDNA), was further evaluated in the presence of heparin, a competing polyanion. Heparin, a large negatively charged polysaccharide found in the extracellular matrix, can disrupt the stability of polyplex nanocarriers by competing for nucleic acid binding. Nanocarriers were formed with 1 μg of DNA at a 1 : 20 w/w ratio and then exposed to varying concentrations of heparin (ranging from 75 ng to 2 μg) and incubated for 60 minutes at 37 °C. Samples were subsequently run on 1% agarose gels and visualized using the same method described previously. Control samples included free pDNA and polyplexes not incubated with heparin. Heparin stability assays were conducted in triplicate, and power analysis was considered for assessing concentration ranges.

Open Access Article. Published on 02 Caxah Alsa 2025. Downloaded on 27/05/2026 6:00:34 PM.
This article is licensed under a Creative Commons Attribution-NonCommercial 3.0 Unported Licence.

### 2.7 Polyplex nanocarriers encapsulation efficiency and *in vitro* release assay

To quantify the encapsulation efficiency of plasmid DNA (pDNA) within the polymeric nanocarriers, the amount of unbound pDNA remaining in the solution was measured. Following the formation of the nanocarriers, a proportional volume of buffer containing a fluorophore was added to the nanocarrier suspension. The mixture was briefly vortexed to ensure thorough mixing and incubated for 5 minutes. Encapsulation efficiency was then determined using Quant-iT dsDNA HS assay kits and a Qubit fluorometer (Invitrogen, USA) according to the manufacturer's instructions. Data replication and sharing policies were followed.

A significant advantage of PBAE-based nanocarrier delivery systems is their ability to achieve sustained release of encapsulated cargo. This controlled release is typically governed by diffusion and degradation processes within the body. In addition to its cationic and biodegradable nature, PBAE efficiently binds with negatively charged pDNA and facilitates its release during polymer degradation. This unique combination of properties results in a nanocarrier system with high encapsulation efficiency and stable gene release. The amount of pDNA released from the nanocarriers was quantified using the Quant-iT™ dsDNA High Sensitivity (HS) assay kit, which utilizes a fluorescent dye specific for double-stranded DNA. Nanocarriers were prepared at DNA-to-polymer weight ratios of 1 : 15, 1 : 20, and 1 : 30 using 1 μg of pDNA per formulation. These complexes were then incubated in PBS at 37 °C to simulate physiological conditions. At predetermined time points (1, 2, 4, 8, 12, 16 and 24 Hours), a fixed volume of each sample was collected, and the Quant-iT™ fluorescent dye was added according to the manufacturer's instructions. Fluorescence was measured using a fluorometer (excitation/emission: 485/530 nm) to determine the concentration of released DNA, which was calculated using a standard curve generated from known DNA concentrations. All measurements were conducted in triplicate, and the average values with standard deviations are presented in Fig. 2C.

### 2.8 Cell culture

In this study, the Jurkat cell line (obtained from the Royan Institute, Iran) was utilized for transfection experiments. The cells were cultured for 24 hours in RPMI-1640 medium supplemented with 1% GlutaMax (Gibco, USA) and 10% fetal bovine serum (FBS), without antibiotics. Cultures were maintained in a humidified atmosphere with 5% $CO_2$ at 37 °C, and transfection experiments were conducted under identical conditions. Cells at passages below 10 were employed to ensure cell viability and efficient transfection. One day prior to transfection, cells were cultured at a density of $1.5 \times 10^5$ cells per ml, resulting in approximately 70% confluency.

For the isolation of peripheral blood mononuclear cells (PBMCs), blood was drawn from a healthy donor using a heparinized syringe. The collected blood was mixed with an equal volume of PBS and gently layered onto Ficoll solution in a falcon tube. The sample was then subjected to density gradient centrifugation at 400*g* for 40 minutes with an increasing speed of 1 and a decreasing speed of 0. The PBMC layer, located between the Ficoll and plasma layers, was carefully extracted. PBMCs were washed in PBS to remove red blood cells and other components, then counted to proceed with T-lymphocyte activation and proliferation.

To activate and expand T cells, the bottom of a well in a 24-well plate was coated with a solution containing anti-CD3 (Miltenybiotec, 130-093-387) and anti-CD28 (Miltenybiotec, 130-093-375) antibodies based on the previous study.[31] For more detail, after 3 hours, the solution was removed, and 1 million PBMCs were added to the well in CTL cell culture medium (containing 44.5% RPMI-1640, 44.5% Click's media, 1% GlutaMax, and 10% FBS without any antibiotics). Within 24 hours, the cells formed small clusters, resembling colonies. On day 1, half of the culture medium was replaced with fresh medium containing 200 IU/ml human IL-2 (R&D Systems). The proliferated T lymphocytes were collected after 5 days and counted to proceed with the transfection steps.

### 2.9 Cellular internalization

Jurkat cells and primary T cells were selected for this gene delivery study. To initiate the experiment, $2 \times 10^5$ cells per well were seeded into 48-well plates. Replication was ensured by conducting the cellular uptake experiments in triplicate. Randomization of samples was not explicitly performed but consistent cell densities and conditions were maintained for reproducibility.

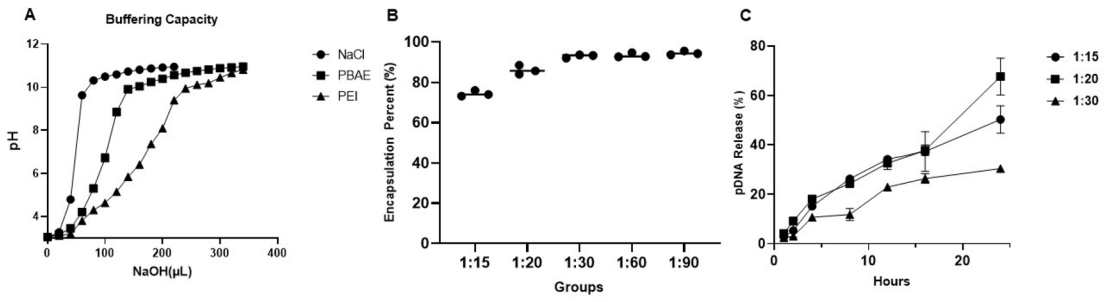


Fig. 2 (A), Buffering capacity analysis showing pH changes in NaCl and compound PBAE and PEI (10 μg of polymer solution with concentration of 100 mg $mL^{-1}$) upon titration with NaOH. Samples were initially adjusted to pH 3 using 1 M HCl and then titrated to pH 11 using 0.1 M NaOH, demonstrating the superior buffering efficiency of compound PBAE. (B), encapsulation efficiency of PBAE nanocarriers at different DNA to polymer weight-to-weight (w/w). (C), release profile of pDNA from nanocarriers over time.


© 2025 The Author(s). Published by the Royal Society of Chemistry

Open Access Article. Published on 02 Caxah Alsa 2025. Downloaded on 27/05/2026 6:00:34 PM.
This article is licensed under a Creative Commons Attribution-NonCommercial 3.0 Unported Licence.

In this study, a cost-effective approach was employed, staining plasmid DNA (pDNA) with Gel-Red, a fluorescent dye targeting nucleic acids such as DNA. A 1 : 20 ratio (1 μg of pDNA to 20 μg of polymer) was utilized, crucial for efficient complex formation between the positively charged polymer and negatively charged DNA. Following a 10 minute incubation for polyplex formation, 20 μL of the nanocarrier solution was added to each well containing Jurkat cells. Blinding was employed during the analysis of flow cytometry results to reduce bias. To maximize cellular uptake, cells were incubated with polyplexes for three hours, as prior studies indicated a gradual increase in polymer nanocarrier absorption within this time frame.[32] A time-course experiment was conducted to evaluate cell uptake efficiency, with cells incubated with nanocarriers for various durations (0.5, 1, 2, 3 hours). This approach identified the optimal incubation time to maximize uptake while minimizing cytotoxic effects. Post-incubation, cells underwent thorough washing to remove unabsorbed nanocarriers two times, ensuring accurate subsequent analyses. The study adhered to cell viability assessments to confirm that experimental conditions did not negatively impact cell health. For T-lymphocyte cells, due to the similar conditions to Jurkat cells, the same proportions, amounts, and incubation times were applied in their study.

Further details included monitoring the fluorescent intensity using flow cytometry and confirming the successful internalization of nanocarriers *via* confocal microscopy. Regular assessments of cell health and morphology, along with optimization of transfection efficiency through varying transfection parameters, were necessary to validate the study's outcomes.

### 2.11 Transfection and gene expression

After PBMCs isolation, to activate T cells, two methods were used: the antibody-based method and the co-culture with artificial antigen-presenting cells (aAPCs) method. The aAPCs-based activation was previously established and worked.[31] Based on the antibody method, the bottom of the cell culture plate was coated with anti-CD3 and anti-CD28 antibodies. These antibodies bind to their respective receptors on the T cell surface, initiating a signaling cascade that triggers T cell activation and proliferation. The coated plates were used to culture T cells in a medium supplemented with interleukin-2 (IL-2), promoting their growth, proliferation, and function. On the third day, the T cells were harvested, centrifuged, and seeded at a density of 200 000 cells per well in a 96-well plate containing Opti-MEM. The synthesized nanocarriers were then added to the cells. After a 3 hours incubation period, half of the supernatant was removed and replaced with an equal volume of CTL medium containing 5% serum. Forty-eight hours post-transfection, the cells were collected and imaged using a fluorescent microscope.

For all transfection experiments, a plasmid encoding enhanced green fluorescent protein (N1-EGFP; Clontech) was used as the reporter gene. The amount of plasmid DNA per well was 1 μg, and it was complexed with the synthesized polymers at weight ratios of 1 : 15, 1 : 20, and 1 : 30 in Opti-MEM reduced-serum medium (100 μL per well in 96-well plates). Jurkat and primary T cells were seeded at a density of 200 000 cells per well. After complex formation (incubation for 30 minutes at room temperature), nanocarrier-pDNA complexes were added directly to the cells. The cells were incubated for 3 hours at 37 °C in a humidified $CO_2$ incubator. Following this, half of the transfection medium was removed and replaced with fresh RPMI 1640 (for Jurkat cells) or CTL medium (for primary T cells), each supplemented with 5% fetal bovine serum (FBS). Cells were further incubated for 48 hours to allow for gene expression.

For the comparator group, transfections were performed using Lipofectamine™ 2000 (Thermo Fisher Scientific) as a benchmark. Lipofectamine-DNA complexes were prepared following the manufacturer's protocol. Briefly, 1 μg of N1-EGFP plasmid was diluted in 50 μL of Opti-MEM and mixed with 2 μL of Lipofectamine 2000 diluted in 50 μL of Opti-MEM. The mixture was incubated for 20 minutes at room temperature to allow complex formation, and then added to the cells in 96-well plates. The remaining steps were identical to the polymer nanocarrier protocol, including the medium replacement and the 48 hours incubation period.

Transfection efficiency was assessed by flow cytometry using a BD FACS Calibur cytometer. GFP expression was quantified in the FL1-H channel and analyzed using forward and side scatter plots for gating. Fluorescence microscopy was also performed to visualize gene expression. All transfection experiments were conducted in three independent biological replicates.

### 2.12 Fluorescence and confocal microscopy

Jurkat and primary T cells were cultured in 48-well plates at a density of $1 \times 10^5$ cells per well, each well containing 350 μl of RPMI-1640 or CTL medium with 10% FBS, and incubated for one day prior to transfection. Replication of imaging experiments was achieved by preparing three independent samples. The preparation of nanocarriers with an N/P ratio of 1 : 20 which involved labeling nucleic acid with Gel-Red, was done. After incubating the cells with these nanocarriers for three hours, the medium was replaced.

Confocal microscopy was employed to assess nanocarrier internalization and the localization of Gel-Red-labeled nucleic acid. Imaging was performed using a Leica TCS SP8 laser scanning confocal spectral microscope (Leica Microsystems Heidelberg, Manheim, Germany), equipped with argon and HeNe lasers on an inverted Leica DMi8 S platform microscope. A 40× objective lens with a numerical aperture of 1.4 was utilized, and laser lines of 405, 488, 528, and 633 nm were employed. An acoustic beam splitter was used to separate the light, with emission detection ranges set between 430–410 nm and 660–645 nm. Additionally, fluorescence imaging was conducted using an Olympus IX71 fluorescence microscope (Olympus Life Science, Japan), capable of detecting radiation at wavelengths of 420, 520, and 590 nm. This qualitative analysis confirmed the successful internalization of the polymeric nanocarriers and the localization of the labeled nucleic acid within the cells.

Open Access Article. Published on 02 Caxah Alsa 2025. Downloaded on 27/05/2026 6:00:34 PM.
This article is licensed under a Creative Commons Attribution-NonCommercial 3.0 Unported Licence.

### 2.13 Cell viability studies

In addition to assessing cell viability through propidium iodide (PI) staining and flow cytometry, the viability of primary T cells was evaluated using the Multiskan Spectrum (Thermo Scientific, USA). Replication was ensured by performing cell viability assays in triplicate. All data were analyzed in a blinded fashion to minimize subjective bias. Also, the MTS assay was performed 24 hours post-transfection, adhering to the standard transfection protocol. Specifically, 20 μl of CellTiter reagent was added to each well and incubated for 2.5 hours at 37 °C. Absorbance was then measured using a plate reader at a wavelength of 490 nm. Background absorbance from the medium and reagent was subtracted, and the resulting values were normalized to the absorbance of untreated cells. In this experiment, the control group consisted of untreated cells, assumed to represent 100% viability. A power analysis was performed to validate the sample size required for detecting significant changes in viability across experimental conditions. Statistical analysis was conducted to confirm reproducibility and significance. Cell viability (%) was calculated using the following formula:

$$\text{Cell viability (\%)} = [\text{abs(samples)/abs(control)}]\ 100\%$$

Jurkat T lymphocyte cells were cultured in RPMI-1640 medium supplemented with 10% FBS and without any antibiotics. For cytotoxicity evaluation, both PBAE nanocarriers and the polymer alone were prepared at varying concentrations, 1 : 15, 1 : 20 and 1 : 30 DNA/polymer w/w ratio for nanocarrier and just 1 : 30 for polymer, diluted in sodium acetate buffer prior to use. To assess the cytotoxicity of PBAE formulations, Annexin V-FITC/PI staining was employed using a commercial apoptosis detection kit (Invitrogen), following the manufacturer's protocol. Jurkat cells were seeded in 96-well plates at a density of 1 × 105 cells per well and treated with PBAE nanocarriers or polymer-only formulations at indicated concentrations for either 4 or 12 hours. Untreated cells served as negative controls. Following incubation, cells were harvested, washed twice with cold PBS, and resuspended in 1× binding buffer. Subsequently, 2 μL of Annexin V-FITC and 2 μL of propidium iodide were added to each 100 μL cell suspension and incubated for 15 minutes at 40 °C temperature in the dark. Samples were analyzed using a flow cytometer. Fluorescence data were acquired using FL1-H (Annexin V-FITC) and FL3-H (PI) channels after compensation. A total of 10 000 events per sample were recorded, and data analysis was performed using FlowJo™ software.

Cell populations were categorized into four quadrants based on fluorescence intensity: Q1 (Annexin $V^-/PI^+$) indicating necrotic cells, Q2 (Annexin $V^+/PI^+$) representing late apoptotic cells, Q3 (Annexin $V^+/PI^-$) for early apoptotic cells, and Q4 (Annexin $V^-/PI^-$) corresponding to viable cells. Quantitative analysis was conducted to determine the percentage distribution of cell populations across quadrants under different treatment conditions. Comparative evaluation between 4 hours and 12 hours treatment groups was performed to assess time-dependent cytotoxicity. The contribution of the polymer alone to cell death was also examined by applying the same staining protocol and flow analysis to cells treated with equivalent polymer concentrations without nanocarrier formulation.

### 2.14 Statistical analysis

All experimental data are expressed as the mean ± standard deviation (SD) derived from a minimum of three independent replicates. One-way and two-way ANOVA was performed, considering normality and homogeneity assumptions. Statistical analyses between different groups were conducted utilizing one-way ANOVA *via* GraphPad Prism® software. Statistical significance was set at $p$-values less than 0.05. The abbreviations used are as follows: ns indicates no significant differences; $*p < 0.05$; $**p < 0.01$; $***p < 0.001$; $****p < 0.0001$.

## 3. Results

### 3.1 Polymer synthesis and characterization

To deepen our understanding of PBAEs' role in non-viral gene delivery and the influence of various conditions on this process, we revisited the established synthesis protocol. This enabled us to create polymers with diverse properties, hypothesized to be critical for overcoming intracellular barriers. We conducted a thorough characterization of this polymer, focusing on nanoparticle size, zeta potential, and DNA complex stability through gel retardation assays, which are indicative of stable particle formation. Previous studies have examined how the physicochemical properties of PBAEs, influenced by variations in the acrylate backbone and side-chain amino groups, impact gene transfer efficiency.[33,34]

$^1$H NMR analysis was employed to confirm successful synthesis and analyze properties relevant to gene delivery. H-NMR characterization of the monomers used in the polymer synthesis process is shown in ESI Fig. 1.† This technique allowed us to determine the mean repeat unit of the polymer (molecular weight = 287.36 g $mol^{-1}$) by comparing the area ratio between the terminal secondary amine hydrogen peak (1.7 ppm) and the α-carbon hydrogens of the diacrylate repeat units (4.01 ppm). Minor peaks and satellites observed at 2.50 ppm and 3.38 ppm were attributed to trace amounts of DMSO from solvent in the process of H-NMR analysis (Fig. S2†).

Endosomal escape, a crucial step for effective gene delivery, is significantly influenced by a polymer's buffering capacity. This capacity is largely determined by the presence of secondary and tertiary amine groups within the polymer structure, which can readily accept protons at specific pH levels.[35,36] This strong buffering ability enables PBAEs to sequester protons within the endosome, where the pH naturally decreases. This "proton sponge effect" facilitates endosomal escape, which is essential for efficient gene delivery. To assess the buffering capacity of our polymer, we performed acid-base titration and generated titration curves. From these curves, we calculated the buffering capacity by analyzing the percentage of protonated amine groups between pH 7.4 (cytoplasmic pH) and 5.1 (endosomal


© 2025 The Author(s). Published by the Royal Society of Chemistry

Open Access Article. Published on 02 Caxah Alsa 2025. Downloaded on 27/05/2026 6:00:34 PM.
This article is licensed under a Creative Commons Attribution-NonCommercial 3.0 Unported Licence.

pH). Sodium chloride (NaCl), which lacks buffering capacity, served as a reference, showing a vertical slope in the titration curve (Fig. 2A).

### 3.2 Nanocarrier complexation, stability, and releases

Effective DNA delivery requires the formation of small, positively charged nanoparticles that can efficiently bind and protect DNA. To study the complexation between DNA and the synthesized polymer, we prepared nanocarriers at different weight-to-weight ratios (1 : 15, 1 : 20, and 1 : 30). The gel retardation assay showed 100% encapsulation efficiency for all tested formulations (Fig. S3A†).

After determining the optimal ratios, we investigated the time required for complete complexation. Using a 1 : 20 w/w ratio, we incubated the components for various durations (5, 10, 15, and 20 minutes) to find the minimum incubation time necessary for complex formation. Results indicated that 5 minutes was sufficient for complete complexation, but to ensure thorough reaction in subsequent cell studies, we chose a 10 minute incubation period (Fig. S3A†).

Additionally, we evaluated the stability of the nanocarriers in the presence of heparin using a gel retardation assay. Physiological heparin concentrations in blood plasma range from 1–5 U $mL^{-1}$ (0.005–0.025 mg $mL^{-1}$). The size, surface charge, and composition of low molecular weight PBAE nanocarriers can affect their interaction with heparin. To simulate physiological conditions and determine the minimum heparin concentration required for dissociation, we tested various concentrations (0.075, 0.125, 0.25, 0.5, 0.75, 1, and micrograms). Complete dissociation of the polyplexes occurred at heparin doses of 1 μg or higher, indicating effective pDNA condensation by the synthesized polymer and their stability in the presence of physiologically relevant heparin concentrations (Fig. S3B†).

Encapsulation efficiency is a crucial parameter for assessing nanocarrier formulations, particularly in gene transfer experiments. The encapsulation efficiency of various nanocarrier ratios was determined by measuring unencapsulated DNA using highly sensitive Qubit quantification kits for dsDNA strands in the five DNA to polymer w/w ratios (1 : 15, 1 : 20, 1 : 30, 1 : 60, and 1 : 90). Following the polymer-DNA linkage, the nanocarriers exhibited significant pDNA encapsulation efficiency, reaching up to 95% (Fig. 2B). These findings underscore the suitability of the synthesized polymer for producing nanocarriers with high encapsulation efficiency. The cationic nature of the polymer not only provides the necessary surface charge but also effectively traps pDNA within the desired nanocarrier structures. The quantitative results align with the qualitative assessments from the gel retardation test.

The synthesized polymer, being a cationic biodegradable polymer, not only binds efficiently to negatively charged pDNA (as confirmed in previous evaluations) but also releases its cargo over time and degrades. This characteristic provides a nanocarrier delivery system with high encapsulation efficiency and sustained gene release capability. The amount of pDNA released from the nanocarriers was determined using Quant-iT dsDNA HS Qubit quantification assay kits, which utilize an ultrasensitive fluorescent nucleic acid dye for double-stranded DNA. The cumulative release profiles are depicted in Fig. 2C.

To evaluate the stability of the manufactured nanocarriers in an extracorporeal environment, their release pattern was investigated over a 24 hours period. Nanocarriers were prepared at ratios of 1 : 15, 1 : 20, and 1 : 30 with 1 microgram of DNA, and their release was assessed using the highly sensitive Quant-iT dsDNA HS Qubit quantification (Fig. 2C). Each test was performed in triplicate to confirm the results.

### 3.3 Nanocarrier's size, charge, and morphology

Building on prior research involving cationic polymers for DNA delivery, it is evident that the formation of small, positively charged nanoparticles is essential for effective delivery.[37–39] However, an excessively high charge density can result in cytotoxicity.[40] Therefore, achieving an optimal balance for each specific polymer is crucial. Additionally, particle size significantly influences the cellular internalization pathway.[19,39]

In this study, PBAE polyplexes were synthesized using various polymer-to-DNA w/w ratios and characterized for size distribution and surface charge. DLS confirmed a monodisperse size distribution for all polyplexes, irrespective of the specific polymer structure. It is important to note that DLS provides an intensity-weighted hydrodynamic diameter, which may overestimate the size of larger particles in polydisperse samples. To validate the DLS results, TEM and SEM imaging were employed.

As illustrated in Fig. 3A, DLS measurements indicated average particle sizes of 112, 203, and 154 nm for polymer-to-DNA w/w ratios of 1 : 15, 1 : 20, and 1 : 30, respectively. While the average particle size in Lipofectamine 2000 lipid nanoparticles was 151 nm. Size distribution of 1 : 20 PBAE nanocarrier obtain through DLS and depicted in Fig. 3B and C by intensity and volume, respectively. Zeta potential measurements (Fig. 3E) confirmed a positive charge for all nanocarriers, ranging from +23.5 mV to +28.3 mV, respectively. As anticipated, both the size and surface zeta potential of the nanocarriers. Increase on polymer-to-DNA w/w ratios. Analysis revealed a clear trend: both particle size and surface charge potential of the nanocarriers increased with a higher polymer-to-DNA weight ratio, with a significant increase in particle size. However, the increase in the surface charge of the nanocarriers was not significant. The results were obtained after repeating the evaluation five times to ensure accuracy due to the limited amount of polymer relative to the genetic material. Notably, the 1.20 ratio exhibited a larger size than the others, which was consistent across successive repetitions, indicating it was not an anomaly.

Further evaluations were conducted to measure particle size under different conditions. It was observed that nanocarriers undergo size changes after being placed in the cellular environment, which particularly affects suspended and smaller cell lines, thereby reducing cellular entry and gene expression.[19,41–43] For investigating this purpose, three media types—PBS, complete media containing 10% serum, and reduced Opti-MEM—were selected, and particle size was recorded at five

Open Access Article. Published on 02 Caxah Alsa 2025. Downloaded on 27/05/2026 6:00:34 PM.
This article is licensed under a Creative Commons Attribution-NonCommercial 3.0 Unported Licence.

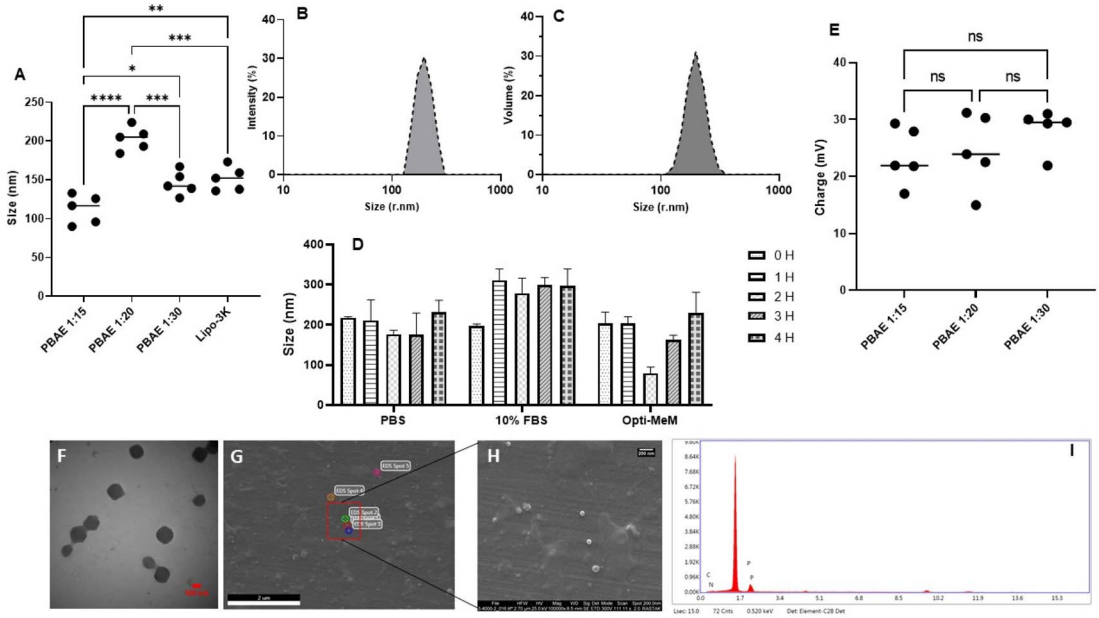


Fig. 3 (A), DLS analysis of the size of nanocarriers at different DNA to polymer ratios. (B and C) Size distribution of nanocarrier based on intensity and volume obtained by DLS(DNA/polymer w/w ratio was 1 : 20) (D), DLS analysis of the size of nanocarriers in the different incubation media (PBS, 10% FBS and reduced Opti-Mem). (E), zeta potential analysis of the surface charge of nanocarriers at different DNA to polymer ratios. (F), TEM image of nanocarriers with a DNA to polymer ratio of 1 : 20. (G), SEM image of nanocarriers. The image provides a detailed view of the surface morphology and structural integrity of the nanocarriers. (H and I), SEM-EDS analysis of nanoparticles. The spectrum identifies the elemental composition of the nanoparticles, confirming the presence of key elements such as carbon (C), nitrogen (N), and phosphorus (P).

different time point intervals using DLS. The results showed no significant size differences between groups at zero time. However, over time, the particle size in the group containing complete media with 10% serum increased by nearly 100 nm, with the increase becoming apparent after one hour. Additionally, the group synthesized in Opti-MEM medium exhibited smaller and more uniform particle sizes compared to the other two groups and was more like the PBS group (Fig. 3D).

For TEM imaging, nanocarriers were synthesized at a w/w ratio of 1 : 20 and imaged under previously described conditions. TEM images confirmed particle sizes of approximately 200 nm or smaller, consistent with the DLS analysis. The nanocarriers exhibited a spherical and uniform morphology, with no observed aggregation (Fig. 3F). SEM-EDS imaging and analysis showed uniform nanocarriers, which were produced by a 1 : 20 w/w ratio. The elemental analysis confirmed the presence of carbon, nitrogen, and phosphorus in the elemental map distribution (Fig. 3G–I).

### 3.4 Nanocarrier internalization

To elucidate the correlation between polymer properties and biological outcomes, we investigated the cellular uptake, transfection efficiency, and cytotoxicity of our nanocarrier formulations. Cellular uptake was tracked using fluorescently labeled pDNA conjugated with Gel-Red dye, with a weight ratio of 1 : 20 (1 μg pDNA). Previous research indicated that nanocarrier endocytosis occurs approximately 2 hours post-cell treatment,[43,44] prompting us to monitor cellular uptake at 0.5, 1, 2, 3, and 4 hours intervals. At each time point, cells were washed twice with PBS to eliminate unbound nanocarriers and residual serum. Cells were then treated with a diluted live/dead green viability kit for 20 minutes.

Confocal microscopy imaging was used for definitive confirmation of intracellular localization, while fluorescent microscope imaging offered a preliminary view of nanocarrier-containing pDNA (Gel-Red) within cells. Despite thorough pre-imaging PBS washes, confocal microscopy was necessary for a more accurate assessment of cellular entry. Jurkat cells were treated with labeled nanocarriers, and after 3 hours, Hoechst dye was used to stain the nucleus, facilitating precise localization of nanocarriers within the cells. Following triple washing and fixation, both two-dimensional and three-dimensional confocal imaging were performed, as depicted in Fig. 4A–D. For a clearer picture of cellular internalization, a single cell was imaged to provide a more detailed and accurate visualization compared to images of larger cell populations.

Flow cytometry analysis demonstrated that approximately 70% of cells exhibited nanocarrier presence after 30 minutes of transfection(Fig. 4E), decreasing to under 60% at 1 hour and about 55% after 3 hours (Fig. 4F). Cell viability analysis indicated that over 70% of cells remained viable 30 minutes post-transfection, with viability decreasing over time.

### 3.5 Transfection efficiency

The transfection efficiency of polymeric nanocarriers in Jurkat cells was evaluated by using 1 μg of pDNA at three different weight ratios (1 : 15, 1 : 20, and 1 : 30). Cells were seeded in 96-well plates, as previously described, and treated with the

 © 2025 The Author(s). Published by the Royal Society of Chemistry

Open Access Article. Published on 02 Caxah Alsa 2025. Downloaded on 27/05/2026 6:00:34 PM.
This article is licensed under a Creative Commons Attribution-NonCommercial 3.0 Unported Licence.

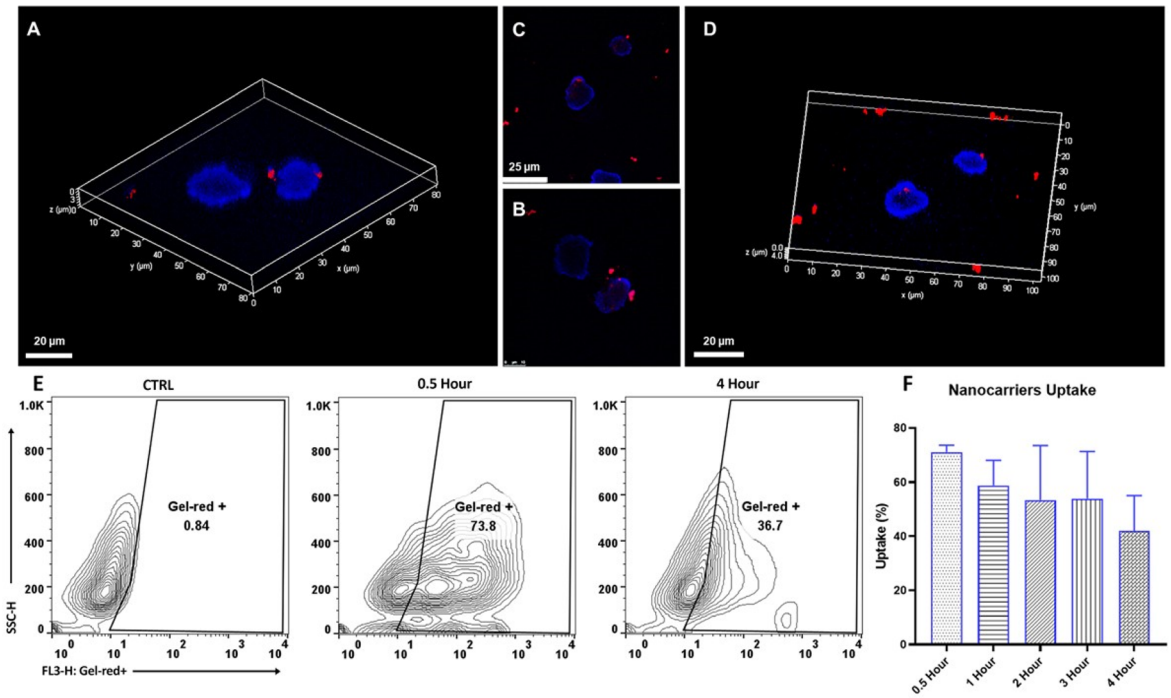


Fig. 4 Confocal microscopy image of Jurkat cells, with nuclei stained blue and nanoparticles highlighted in red, demonstrating efficient cellular uptake and precise intracellular localization of the nanocarriers. (A) and (D) are paired by (B) and (C), respectively. (E), flowcytometry analysis of nanocarrier uptake by jurkat cells. The plots gated based on FL3-H: Ger-red positive cells to SSC-H. (F), the chart depicting the percentage uptake of nanocarriers in the Jurkat cell line over different incubation times (0.5, 1, 2, 3, and 4 hours), highlighting the kinetics of nanoparticle internalization. The uptake percentage refers to the proportion of cells that internalized the nanocarriers, as determined by flow cytometry. The cells were incubated with nanocarriers containing a fluorescent dye.

synthesized nanocarriers. Based on prior studies, a 3 hours incubation period with the nanocarriers was established. After this period, half of the culture medium (transfection medium without serum) was replaced with fresh RPMI 1640 medium containing 5% serum. The cells were then harvested and analyzed *via* Fluorcent microscopy and flow cytometry (Fig. 5A–C). Lipofectamine 2000 served as a gold standard for comparison with the synthetic polymer, following the manufacturer's protocol.

T cells were transfected at a polymer-to-DNA weight ratio of 1 : 20 according to the established protocol. Each group contained 1 μg of plasmid (N1 EGFP), and gene expression was analyzed by flow cytometry 48 hours post-transfection (Fig. 6A–D). The fluorescent intensity indicative of gene expression led to

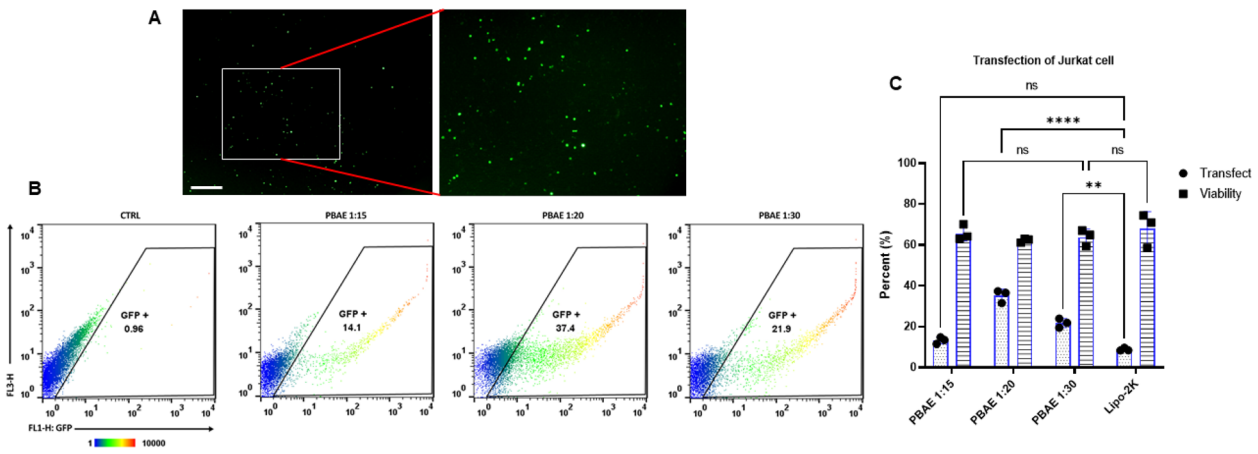


Fig. 5 (A), Fluorescent microscopy images of transfected Jurkat cells. (B), flow cytometry plots representing the transfection efficiency (GFP-positive cells) in Jurkat cells, providing a quantitative measure of gene expression post-transfection. (C), transfection efficiency and viability of Jurkat cells treated with different DNA to polymer ratios (1 : 15, 1 : 20, and 1 : 30) of PBAE, with Lipofectamine 2000 (Lipo-2K) used as a comparison reagent.

Open Access Article. Published on 02 Caxah Alsa 2025. Downloaded on 27/05/2026 6:00:34 PM.
This article is licensed under a Creative Commons Attribution-NonCommercial 3.0 Unported Licence.

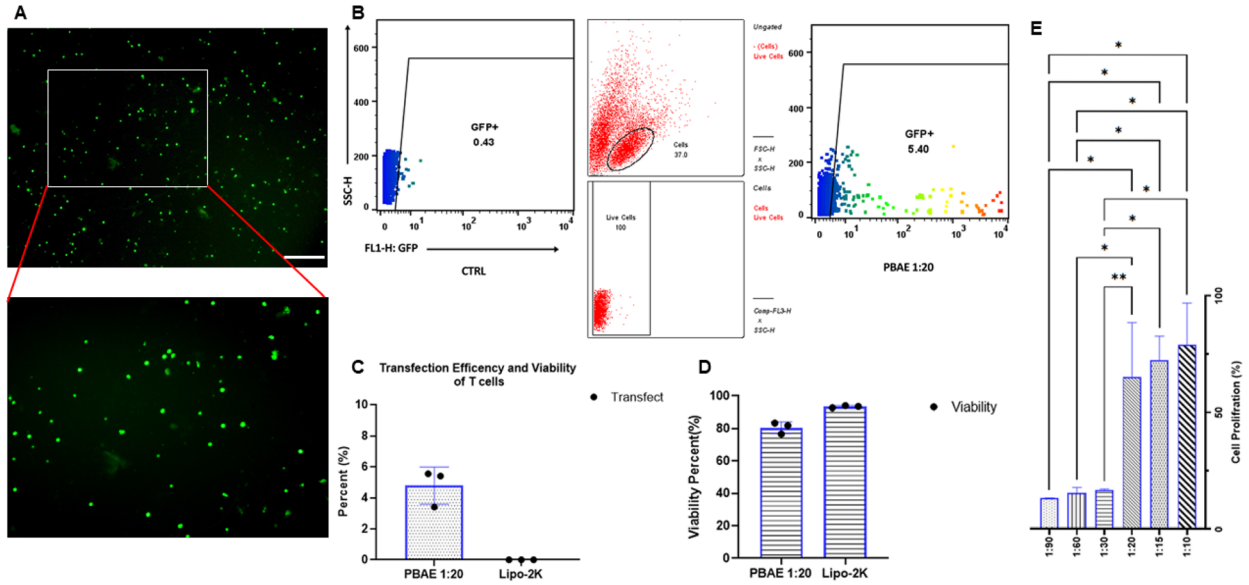


Fig. 6 (A), Fluorescent microscopy images of transfected T cells, with green fluorescence indicating successful gene transfection. (B), flow cytometry results showing the transfection efficiency in T cells, demonstrating the effectiveness of the gene delivery method. (C and D), transfection efficiency and viability of primary T cells treated with a DNA-to-polymer ratio of 1 : 20, compared to Lipo-2K. (E), MTS assay analysis of T cells treated with different DNA to polymer ratios of PBAE nanocarriers, illustrating the impact on cell proliferation and viability.

an upward shift in the analysis plots, with gating performed based on the FL1-H: GFP to SSC-H channels (Fig. 6B). For comparison, cells were also transfected using Lipofectamine 2000, following the transfection protocol. Gene expression in these cells was likewise analyzed 48 hours post-transfection, with plots showing similar upward shifts. Fluorescent microscopy images demonstrated the expression of the green fluorescent protein (N1-EGFP) gene in Jurkat (Fig. 5A) and T cells (Fig. 6A).

### 3.6 Polymer and nanocarrier cytotoxicity

Cell viability, serving as an indicator of cytotoxicity, was assessed using the MTS assay method. The evaluation specifically highlighted the T cell group treated with nanocarriers, using six w/w ratios of polymer to genetic material (1 : 10, 1 : 15, 1 : 20, 1 : 30, 1 : 60, and 1 : 90) with a constant 1 μg of pDNA. The results showed a significant decrease in cell viability at higher polymer weight ratios (Fig. 6E).

Notably, in the low polymer weight ratio group, cell viability was from 65% to 75% at a weight ratio of 1 : 10, 1 : 15, and 1 : 20. However, in the medium and high polymer groups, a sharp decrease in cell proliferation was observed. At a weight ratio of 1 : 30, viability dropped to 25% and remained around 20% at 1 : 60.

In addition above analysis, cytotoxic effects of PBAE nanocarriers and the polymer alone were systematically evaluated in Jurkat cells through annexin V-propidium iodide staining and flow cytometry analysis. The study revealed a significant decline in cell viability with increasing concentrations of PBAE, accompanied by a concomitant rise in the necrotic population. This trend was further amplified with prolonged exposure durations, as cells treated for 12 hours exhibited more pronounced reductions in viability compared to those exposed for 4 hours. Notably, the early apoptotic population remained relatively low across all treatment groups, while the necrosis rate increased proportionally with PBAE concentration. These findings suggest that PBAE nanocarriers predominantly induce necrotic cell death rather than apoptosis. In the "Only polymer" condition, similar trends were observed, although the reduction in cell viability and induction of apoptosis were more pronounced at a PBAE ratio of 1 : 30. This indicates that the polymer itself contributes to cytotoxicity but exerts a less potent effect when integrated into PBAE nanocarriers.

Flow cytometry scatter plots provided further insights into the distribution of cell populations based on Annexin V (FL1-H) and PI (FL3-H) staining. Each plot was divided into four quadrants: Q1 representing necrotic cells, Q2 indicating late apoptosis, Q3 corresponding to early apoptotic cells, and Q4 signifying viable cells. In the untreated control group, the majority of cells were localized in Q4, reflecting high viability. However, as the PBAE concentration increased, there was a marked redistribution of cells from Q4 to Q1 and Q2, particularly at higher concentrations and extended exposure times. This shift underscores the dose- and time-dependent cytotoxic effects of PBAE.

Finally, the data indicate that PBAE induces both apoptosis and necrosis in Jurkat cells, with necrosis being the predominant mode of cell death. While the rate of apoptosis remained relatively stable across treatment groups, higher PBAE concentrations significantly increased necrosis rates, an effect further enhanced by prolonged exposure. These results suggest that PBAE primarily activates necrotic pathways rather than apoptotic ones. Such findings not only deepen our understanding of the biological mechanisms underlying PBAE-


© 2025 The Author(s). Published by the Royal Society of Chemistry

Open Access Article. Published on 02 Caxah Alsa 2025. Downloaded on 27/05/2026 6:00:34 PM.
This article is licensed under a Creative Commons Attribution-NonCommercial 3.0 Unported Licence.

induced cytotoxicity but also highlight its potential applications in therapeutic contexts, particularly in scenarios where controlled cell death is desirable. By elucidating the interplay between necrosis and apoptosis induced by PBAE, this study provides a foundation for the continued optimization and development of PBAE-based systems for drug delivery and other biomedical applications.

# 4. Discussion

Low molecular weight PBAE polymer has garnered significant interest in the field of gene delivery due to their unique properties and efficiency.[45] Low molecular weight PBAEs are generally more biocompatible compared to their higher molecular weight counterparts.[46] This reduces cytotoxicity and makes them safer for use in gene delivery applications. The polymer can more easily penetrate cell membranes due to their smaller size, leading to higher transfection efficiency.[47] Low molecular weight PBAEs often show higher DNA complexation efficiency, which is crucial for effective gene delivery. This polymer can be used to deliver a wide range of genetic materials, including plasmid DNA and CRISPR/Cas9 components.[46]

PBAEs exhibit significantly lower cytotoxicity compared to polyethyleneimine (PEI),[33] and their typical formulation at 20 w/w (weight by weight) results in a much higher total buffering capacity for PBAE-based particles compared to PEI formulations at a 1/1 ratio. For example, the PBAE with the lowest buffering capacity per mass unit can buffer 1.7 mmol H+/g. However, due to the 20-fold higher polymer content in PBAE formulations compared to PEI, 20 w/w PBAE particles can buffer more protons than 1 w/w PEI.

The molecular weight range of synthesized polymer is approximately from 3 to 3.5 k-Daltons, which covers small-to medium-sized polymer chains (Fig. S2†). This indicates that the majority of the polymer sample has a molecular weight centered around 3 to 3.5 Daltons, suggesting a relatively consistent polymerization process.

The ratio of polymer to genetic material is crucial as it influences the efficiency of gene delivery into the cells. Too little polymer may not form stable polyplexes, while too much can cause toxicity and hinder transfection efficiency. Thus, these specific ratios were selected to find a balance between stability and biocompatibility.

After complexation, the size of the nanoparticles, their surface charge, and also their size changes under different incubation environments (PBS, complete cell culture, and reduced Opti-MEM media) were investigated (Fig. 3D). Nanoparticle size remains relatively consistent across different incubation times, with minor variations. This indicates that PBS maintains the stability of nanoparticles over time. While nanoparticle size increases significantly in cell culture media (FBS 10%), especially at longer incubation times. This suggests that proteins in FBS interact with nanoparticles, possibly leading to agglomeration or changes in surface characteristics. In the Opti-MEM incubation medium, nanoparticle size shows variability, with a notable increase at 4 hours of incubation. This could be due to the components in Opti-MEM interacting with the nanoparticles, affecting their dispersion and stability. The differences in nanoparticle sizes across various environments highlight the importance of the incubation medium in determining nanoparticle behavior. In PBS, nanoparticles maintain their size, suggesting good stability. However, in biological media like FBS, interactions with proteins and other components cause variations in size, which can impact the nanoparticles' functionality in applications such as drug delivery and gene therapy. However, the results indicate that the Opti-Mem medium, due to the lack of serum and additional proteins, was able to function like PBS medium. This result emphasizes the need to carefully consider the incubation environment when developing nanoparticle-based systems, as it significantly influences their stability and performance. Further studies may explore the mechanisms behind these interactions and develop strategies to optimize nanoparticle formulations for desired applications.

The encapsulation rate remains consistently high across all groups, indicating efficient DNA encapsulation regardless of the ratio used. DNA release increases gradually over time (Fig. 2C), demonstrating a sustained release profile that is beneficial for gene delivery applications (almost all of the release is very small in the first 3 hours). Significant differences in particle size are noted between the groups, with PBAE 1 : 30 showing the largest size and Lipo-2K the smallest. Statistical significance is indicated by asterisks, showing the variations are meaningful. Surface charge is relatively consistent across the formulations, with no significant differences, which is crucial for understanding nanoparticle stability and interaction with cellular membranes.

The SEM-EDS result shows a surface with several spherical particles, which are likely the PBAE nanoparticles. A smaller peak around 0.25 keV, indicating the presence of carbon (C) as a primary component. The second peak is around 0.5 keV, indicating the presence of nitrogen (N) and two peaks are around 2 keV, indicating the presence of phosphorus (P). The SEM image reveals that the nanoparticles are spherical, which is consistent with typical PBAE nanoparticles (Fig. 3G–I).

The EDS spectrum confirms that the nanoparticles primarily contain carbon, nitrogen, and phosphorus. These elements are consistent with the expected composition of PBAE polymer and any encapsulated substances.

The confocal microscopy images provide valuable insights into the behavior and efficiency of the nanocarriers in gene delivery applications (Fig. 4). The red fluorescence within the cells indicates successful internalization of the nanocarriers. This suggests that the nanocarriers efficiently penetrate the cell membrane and deliver their cargo into the intracellular environment. The close proximity of the red nanocarriers to the blue-stained nuclei highlights the potential for effective gene transfer. The nanocarriers' localization near the nucleus is crucial for gene delivery, as it facilitates the entry of genetic material into the nucleus for transcription and subsequent gene expression. These images vividly demonstrate the capability of the designed nanocarriers to penetrate cells and localize near the nuclei. This efficient internalization and localization are critical factors for the success of gene delivery applications. The

Open Access Article. Published on 02 Caxah Alsa 2025. Downloaded on 27/05/2026 6:00:34 PM.
This article is licensed under a Creative Commons Attribution-NonCommercial 3.0 Unported Licence.

image serves as compelling evidence of the potential utility of these nanocarriers in targeted gene therapy.

The uptake percentage is the highest at approximately 75%, indicating a rapid initial uptake of nanocarriers by the Jurkat cells (Fig. 4F). The high uptake at 0.5 hours demonstrates that the nanocarriers are quickly internalized by the Jurkat cells. This rapid uptake is beneficial for applications requiring swift cellular delivery. The decrease and subsequent plateau indicate that after the initial burst, the cells might reach a saturation point or adjust their internalization mechanisms. This stabilization suggests that the maximum uptake capacity is achieved early and maintained over time. These findings are crucial for optimizing incubation times in gene and drug delivery applications. Knowing that significant uptake occurs within the first hour allows researchers to design efficient delivery protocols without prolonged incubation, which could reduce potential cytotoxic effects and improve overall efficiency.

The PBAE polymer at all three tested ratios (1 : 15, 1 : 20, 1 : 30) show a consistent transfection efficiency 14.1, 37.4 and 21.9 respectively (Fig. 5B and C). This consistency suggests that the ratio variations of PBAE to DNA do not significantly impact the transfection efficiency within the tested range. However, among the studied groups, the 1 : 20 ratio was more able to transfect cells than the others. Interestingly, the Lipo-2K control showed a transfer efficiency of less than 5%. The viability of Jurkat cells remains stable at around 60% for all conditions, indicating that the PBAE polymer do not induce additional cytotoxicity compared to the commercial standard Lipo-2K. The data presented in this bar graph highlight the potential of PBAE polymer for gene delivery in Jurkat cells, maintaining consistent transfection efficiency while preserving cell viability. The comparable viability across all conditions, including the commercial standard Lipo-2K, supports the biocompatibility of PBAE polymer. Zhou and colleagues conducted a study to transfect Jurkat cells using the polymer nanocarrier PBAE. It was found that transfection occurred only in cells pre-treated with polybrene before exposure to the manufactured nanocarriers. Polymers with a molecular weight of less than 7 kDa were used, and approximately 30% transfection of Jurkat cells was achieved. Additionally, when their results were compared with those obtained using Lipofectamine, it was demonstrated that the Lipofectamine-treated group exhibited 8 times lower transfection efficiency. In contrast, our results showed that Jurkat cells transfected with polymer nanocarriers of less than 5 kDa molecular weight achieved approximately 37% transfection, which was four times higher than the Lipofectamine-treated group. Notably, polybrene treatment was not employed in this study.[48]

The transfection efficiency of PBAE at a 1 : 20 weight ratio is about 5% in primary T cells (Fig. 6B and C). While this is not very high, it indicates that PBAE does facilitate some level of gene transfer into T cells. The viability of T cells transfected with PBAE at this ratio is also around 5%, suggesting that the transfection process may significantly affect cell viability. However, there is some discrepancy, as the viability for PBAE 1 : 20 and Lipo-2K should be significantly different. These observations underscore the need for further optimization in the use of PBAE for gene transfection in T cells to enhance both transfection efficiency and cell viability. Smith *et al.* established the potential of nanoparticle-mediated T-cell programming as a practical and low-cost treatment for cancer. The article presents a novel approach to cancer treatment by programming patient-derived T cells to recognize and combat tumor cells using CAR T cell. A PBAE polymeric nanocarrier was designed, and by attaching an anti-CD3 antibody to its surface, more effective binding to the target cells (T cells) was achieved. The results demonstrated that approximately 3% of T lymphocytes were transfected using the designed nanocarriers. In contrast, in our study, the percentage of transfected cells was increased to over 5% without using any specific antibody on the nanocarriers.[6] In another study, Olden *et al.* synthesized cationic polymers that were branched and consisted of the pHEMA-g-pDMAEMA structure. These polymer nanocarriers, with a size of less than 150 nm and a zeta potential of approximately 30 mV, were able to transfect nearly 50% of Jurkat cells in serum-free medium. However, this transfection efficiency was reduced to 18% in T cells. While their study utilized branched polymer, the results from transfection studies with linear polymer indicated that these types of polymer was unable to transfect cells. In contrast, our study focused on the synthesis of linear polymer and successfully achieved the desired transfection rate using this linear polymer. The synthesis of these linear polymer was found to be not only simpler but also more cost-effective.[49]

The difference in transfection efficiency between Jurkat cells and primary T cells can be attributed to several factors. Jurkat cells are immortalized and have higher metabolic activity and more permissive membrane properties, making them generally easier to transfect.[50] In contrast, primary T cells are more physiologically relevant but significantly harder to transfect due to their rigid cytoskeleton, lower endocytic activity, and stronger homeostatic mechanisms that resist foreign material uptake. The internalization pathways of nanoparticles also differ between these two cell types. Moreover, Lipofectamine 2000 and polymeric nanocarriers utilize different mechanisms for transfection, which could explain their varying efficiencies in different cell types.[51–53]

The cell proliferation rate is highest at the 1 : 15 and 1 : 10 weight ratios of DNA to PBAE (Fig. 6E). This suggests that lower amounts of PBAE to DNA relative promote better cell growth and proliferation. These ratios likely provide an optimal environment for T cells, balancing efficient gene transfection with minimal cytotoxic effects. While the reduced proliferation rates at higher PBAE ratios (1 : 90, 1 : 60) could be due to several factors, including potential cytotoxicity or suboptimal conditions for cell growth, this indicates that an excess of DNA might inhibit cell proliferation, possibly due to overloading the cells' metabolic and regulatory systems. Ratios of 1 : 15 and 1 : 20 are particularly effective, providing a useful guideline for future gene delivery experiments and potential therapeutic applications. Our results revealed that necrosis is the predominant mode of cell death at higher PBAE concentrations, particularly at the 1 : 30 ratio, suggesting that membrane disruption may indeed play a significant role, likely due to the high cationic


© 2025 The Author(s). Published by the Royal Society of Chemistry

Open Access Article. Published on 02 Caxah Alsa 2025. Downloaded on 27/05/2026 6:00:34 PM.
This article is licensed under a Creative Commons Attribution-NonCommercial 3.0 Unported Licence.

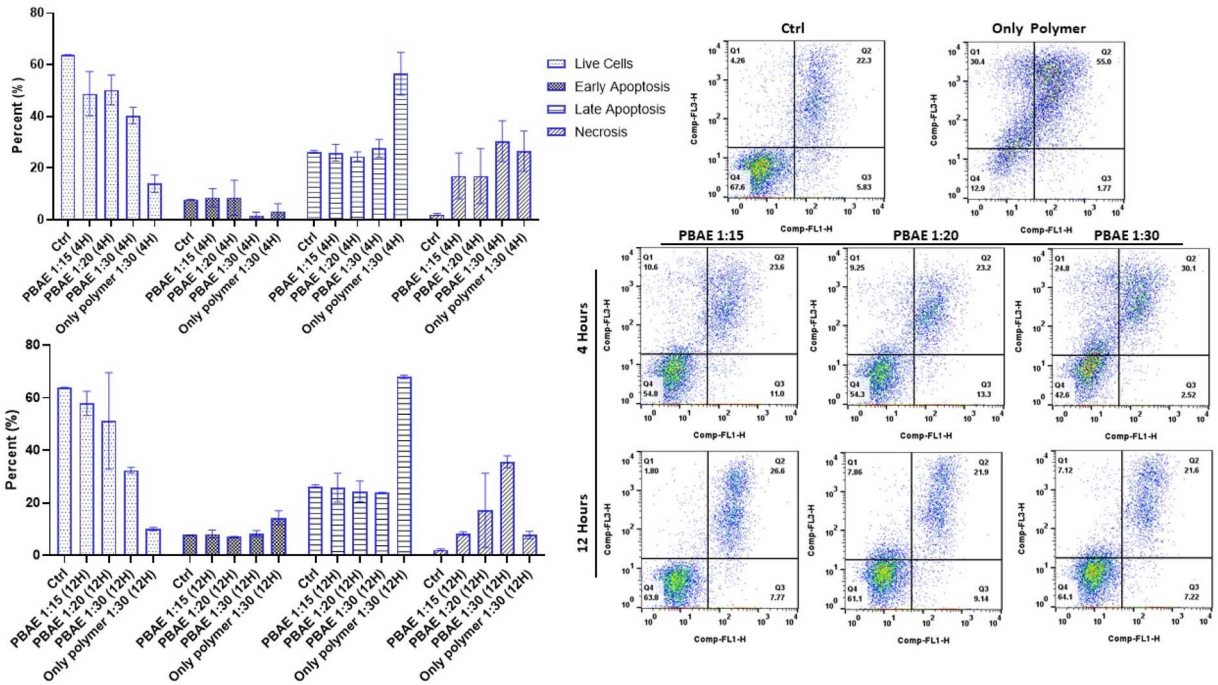


Fig. 7 Assessment of PBAE-induced cytotoxicity in Jurkat cells *via* Annexin V/Propidium Iodide (PI) staining and flow cytometry. Jurkat cells were treated with PBAE nanocarriers and the polymer alone at varying concentrations (1 : 15, 1 : 20, 1 : 30) for 4 and 12 hours. Bar graphs (left) depict the quantification of live cells, early apoptotic cells, late apoptotic cells, and necrotic cells, highlighting a dose- and time-dependent decrease in cell viability and a predominant induction of necrosis over apoptosis. Representative flow cytometry scatter plots (right) show the distribution of cell populations based on Annexin V (FL1-H) and PI (FL3-H) staining. Quadrants: Q1—necrosis (Annexin $V^-/PI^+$), Q2—late apoptosis (Annexin $V^+/PI^+$), Q3—early apoptosis (Annexin $V^+/PI^-$), Q4—viable cells (Annexin $V^-/PI^-$). A marked shift from Q4 to Q1 and Q2 with increasing PBAE concentration and exposure time indicates that necrosis is the dominant mode of cell death induced by PBAE treatment.

charge density of the polymer (Fig. 7A–C). Interestingly, the early apoptotic population remained relatively low across all treatment groups, further supporting the hypothesis that membrane destabilization rather than apoptotic signaling pathways may underlie the observed cytotoxicity.

## 5. Conclusion

This study presents a comprehensive evaluation of low molecular weight PBAE polymer in the context of non-viral gene delivery, with a specific focus on Jurkat and T cells. The successful synthesis and characterization of this polymer, combined with detailed analysis of their size, charge, morphology, and biological performance, highlight their potential as effective vectors for gene therapy. By exploring the cellular uptake, transfection efficiency, and cytotoxicity of PBAE nanocarriers, we established their ability to efficiently deliver genetic material into both Jurkat and primary T cells, about 37% and 5%, respectively. The high transfection efficiency observed, particularly at the optimized DNA-to-polymer ratios, demonstrates the efficacy of PBAE nanocarriers in facilitating gene expression without significantly compromising cell viability.

One of the key advancements of this research lies in the application of PBAE nanocarriers to T cells, which are central to cancer immunotherapy. The ability to effectively transfect T cells with therapeutic genes opens new avenues for enhancing their anti-tumor activity, offering a promising approach for cancer treatment. The results indicate that the optimized PBAE formulations can achieve high levels of gene expression while maintaining cell viability, making them suitable for potential therapeutic applications.

Furthermore, the study underscores the significance of balancing polymer concentration to minimize cytotoxicity while maximizing transfection efficiency. This balance is crucial for developing safe and effective gene delivery systems that can be used in clinical settings. The findings also highlight the importance of understanding the interactions between nanocarriers and the cellular environment to improve the design of next-generation gene delivery vectors.

## Data availability

The data supporting the findings of this study are available within the article and its ESI materials.† Additional data that support the findings of this study are available from the corresponding author upon reasonable request.

## Author contributions

Alireza Gharatape: conceptualization, investigation, methodology, literature search, data curation, visualization, writing–

Open Access Article. Published on 02 Caxah Alsa 2025. Downloaded on 27/05/2026 6:00:34 PM.
This article is licensed under a Creative Commons Attribution-NonCommercial 3.0 Unported Licence.

original draft, writing–review & editing. Ali Sayadmanesh: methodology, data curation, visualization, writing–review & editing. Hamid Sadeghi-Abandansari: formal analysis, investigation, writing–review & editing. Hossein Ghanbari: formal analysis, investigation, writing–review & editing. Mohsen Basiri: conceptualization, formal analysis, funding acquisition, investigation, methodology, project administration, resources, supervision, writing–review & editing. Reza Faridi-Majidi: conceptualization, formal analysis, funding acquisition, investigation, project administration, resources, supervision, writing–review & editing. All authors have read and agreed to the published version of the manuscript.

## Conflicts of interest

There is no conflict of interests to declare.

## Acknowledgements

This work received funding from the Tehran University of Medical Sciences under grant code 1402-1-148-65099.

## References

1 L. Barazzuol, R. P. Coppes and P. van Luijk, *Mol. Oncol.*, 2020, **14**, 1538–1554.
2 D. T. Debela, S. G. Muzazu, K. D. Heraro, M. T. Ndalama, B. W. Mesele, D. C. Haile, S. K. Kitui and T. Manyazewal, *SAGE Open Med.*, 2021, **9**, 1–10.
3 A. R. Kumar, A. R. Devan, B. Nair, B. S. Vinod and L. R. Nath, *Mol. Biol. Rep.*, 2021, **12**, 1–21.
4 K. Kaur and G. L. Khatik, *Curr. Cancer Ther. Rev.*, 2020, **16**, 62–69.
5 N. N. Parayath, S. B. Stephan, A. L. Koehne, P. S. Nelson and M. T. Stephan, *Nat. Commun.*, 2020, **11**, 6080.
6 T. T. Smith, S. B. Stephan, H. F. Moffett, L. E. McKnight, W. Ji, D. Reiman, E. Bonagofski, M. E. Wohlfahrt, S. P. Pillai and M. T. Stephan, *Nat. Nanotechnol.*, 2017, **12**, 813–820.
7 T. Haslauer, R. Greil, N. Zaborsky and R. Geisberger, *Int. J. Mol. Sci.*, 2021, **22**, 8996.
8 F. Wang, Y. Huang, J. Li, W. Zhou and W. Wang, *Cell. Oncol.*, 2024, **47**, 1537–1560.
9 A. Moretti, M. Ponzo, C. A. Nicolette, I. Y. Tcherepanova, A. Biondi and C. F. Magnani, *Front. Immunol.*, 2022, **13**, 867013.
10 G. I. Ellis, N. C. Sheppard and J. L. Riley, *Nat. Rev. Genet.*, 2021, **22**, 427–447.
11 J. A. Myers and J. S. Miller, *Nat. Rev. Clin. Oncol.*, 2021, **18**, 85–100.
12 C. Liu, M. Yang, D. Zhang, M. Chen and D. Zhu, *Front. Immunol.*, 2022, **13**, 961805.
13 I. S. Pinto, R. A. Cordeiro and H. Faneca, *J. Controlled Release*, 2023, **353**, 196–215.
14 A. Gharatape, B. Amanzadi, F. Mohamadi, M. Rafieian and R. Faridi-Majidi, *Nanomedicine*, 2024, **19**, 2655–2678.
15 H. Dabiri, P. Safarzadeh Kozani, M. Habibi Anbouhi, M. Mirzaee Godarzee, M. H. Haddadi, M. Basiri, V. Ziaei, M. Sadeghizadeh and E. H. Saffar, *Biomark. Res.*, 2023, **11**, 67.
16 J. B. Sandbrink, E. C. Alley, M. C. Watson, G. D. Koblentz and K. M. Esvelt, *Gene Ther.*, 2023, **30**, 407–410.
17 M. Sainz-Ramos, I. Gallego, I. Villate-Beitia, J. Zarate, I. Maldonado, G. Puras and J. L. Pedraz, *Int. J. Mol. Sci.*, 2021, **22**, 7545.
18 Z. Zhao, A. C. Anselmo and S. Mitragotri, *Bioeng. Transl. Med.*, 2022, **7**, e10258.
19 A. Gharatape, H. Sadeghi-Abandansari, A. Seifalian, R. Faridi-Majidi and M. Basiri, *J. Mater. Chem. B*, 2024, **12**, 3356–3375.
20 J. J. Green, G. T. Zugates, R. Langer and D. G. Anderson, *Methods Mol. Biol.*, 2009, 53–63.
21 M. J. B. Sadeqi Nezhad, *Bioengineering*, 2023, **120**, 95–113.
22 T. M. D. Le, A.-R. Yoon, T. Thambi and C.-O. Yun, *Front. Immunol.*, 2022, **13**, 826876.
23 L. Ke, P. Cai, Y. L. Wu and X. Chen, *Adv. Ther.*, 2020, **3**, 1900213.
24 J. Long, Y. Wang, X. Jiang, J. Ge, M. Chen, B. Zheng, R. Wang, M. Wang, M. Xu and Q. Ke, *Adv. Healthcare Mater.*, 2024, 2304615.
25 X. Gao, Z. Jin, X. Tan, C. Zhang, C. Zou, W. Zhang, J. Ding, B. C. Das, K. Severinov and I. I. Hitzeroth, *J. Controlled Release*, 2020, **321**, 654–668.
26 D. Zhu, H. Shen, S. Tan, Z. Hu, L. Wang, L. Yu, X. Tian, W. Ding, C. Ren and C. Gao, *Mol. Ther.*, 2018, **26**, 2443–2455.
27 K. M. Luly, H. Yang, S. J. Lee, W. Wang, S. D. Ludwig, H. E. Tarbox, D. R. Wilson, J. J. Green and J. B. Spangler, *Int. J. Nanomed.*, 2022, **17**, 4469.
28 M. Navalón-López, A. Dols-Perez, S. Grijalvo, C. Fornaguera and S. Borrós, *Nanoscale Adv.*, 2023, **5**, 1611–1623.
29 Z. Zhang, L. Wang, X. Ma and H. Wang, *J. Pharm. Anal.*, 2023, **14**, 100922.
30 N. Parayath, S. Hao, S. Stephan, A. Koehne, C. Watson and M. Stephan, *J. Controlled Release*, 2021, **339**, 553–561.
31 A. Sayadmanesh, M. Azadbakht, K. Yari, A. Abedelahi, H. Shafaei, D. Shanehbandi, B. Baradaran and M. Basiri, *Cell J.*, 2023, **25**, 674–687.
32 A. Gharatape, H. Sadeghi-Abandansari, H. Ghanbari, M. Basiri and R. Faridi-Majidi, *Nanomedicine*, 2025, **20**(2), 125–139.
33 J. Zhang, X. Cai, R. Dou, C. Guo, J. Tang, Y. Hu, H. Chen and J. Chen, *Mol. Ther. Nucleic Acids*, 2023, **32**, 568–581.
34 J. C. Sunshine, D. Y. Peng and J. J. Green, *Mol. Pharm.*, 2012, **9**, 3375–3383.
35 Q. Yang, Y. Dong, X. Wang, Z. Lin, M. Yan, W. Wang, A. Dong, J. Zhang, P. Huang and C. Wang, *Macromol. Biosci.*, 2021, **21**, 2100025.
36 E. Haladjova, V. Chrysostomou, M. Petrova, I. Ugrinova, S. Pispas and S. Rangelov, *Macromol. Biosci.*, 2021, **21**, 2000352.
37 M. J. Mitchell, M. M. Billingsley, R. M. Haley, M. E. Wechsler, N. A. Peppas and R. Langer, *Nat. Rev. Drug Discovery*, 2021, **20**, 101–124.


© 2025 The Author(s). Published by the Royal Society of Chemistry

Open Access Article. Published on 02 Caxah Alsa 2025. Downloaded on 27/05/2026 6:00:34 PM.
This article is licensed under a Creative Commons Attribution-NonCommercial 3.0 Unported Licence.

38 W. Ho, M. Gao, F. Li, Z. Li, X. Q. Zhang and X. Xu, *Adv. Healthcare Mater.*, 2021, **10**, 2001812.
39 C. He, Y. Hu, L. Yin, C. Tang and C. Yin, *Biomaterials*, 2010, **31**, 3657–3666.
40 H. J. Vaughan, J. J. Green and S. Y. Tzeng, *Adv. Mater.*, 2020, **32**, e1901081.
41 T. Lima, K. Bernfur, M. Vilanova and T. Cedervall, *Sci. Rep.*, 2020, **10**, 1129.
42 K. Obst, G. Yealland, B. Balzus, E. Miceli, M. Dimde, C. Weise, M. Eravci, R. Bodmeier, R. Haag, M. Calderón, N. Charbaji and S. Hedtrich, *Biomacromolecules*, 2017, **18**, 1762–1771.
43 P. M. Perrigue, R. A. Murray, A. Mielcarek, A. Henschke and S. E. Moya, *Pharmaceutics*, 2021, **13**, 770.
44 N. Oh and J. H. Park, *Int. J. Nanomed.*, 2014, **9**, 51–63.
45 A. A. Eltoukhy, D. J. Siegwart, C. A. Alabi, J. S. Rajan, R. Langer and D. G. Anderson, *Biomaterials*, 2012, **33**, 3594–3603.
46 J. Ding, H. Zhang, T. Dai, X. Gao, Z. Yin, Q. Wang, M. Long and S. Tan, *Pharmaceutics*, 2024, **16**, 213.
47 J. C. Sunshine, S. B. Sunshine, I. Bhutto, J. T. Handa and J. J. Green, *PLoS One*, 2012, **7**, e37543.
48 N. Zhao, J. Qi, Z. Zeng, P. Parekh, C.-C. Chang, C.-H. Tung and Y. Zu, *J. Controlled Release*, 2012, **159**, 104–110.
49 B. R. Olden, Y. Cheng, J. L. Yu and S. H. Pun, *J. Controlled Release*, 2018, **282**, 140–147.
50 C. Ledderose, T. Woehrle, S. Ledderose, K. Strasser, R. Seist, Y. Bao, J. Zhang and W. G. Junger, *Purinergic Signalling*, 2016, **12**, 439–451.
51 J. C. Charpentier and P. D. King, *Cell Commun. Signal.*, 2021, **19**, 92.
52 H. Yin, R. L. Kanasty, A. A. Eltoukhy, A. J. Vegas, J. R. Dorkin and D. G. Anderson, *Nat. Rev. Genet.*, 2014, **15**, 541–555.
53 G. Chen, I. Roy, C. Yang and P. N. Prasad, *Chem. Rev.*, 2016, **116**, 2826–2885.

© 2025 The Author(s). Published by the Royal Society of Chemistry